J Mater Sci (2009) 44:4677–4682
DOI 10.1007/s10853-009-3716-0

Tunable ZnO nanostructures for ethanol sensing

Wei-De Zhang · Wen-Hui Zhang · Xue-Yong Ma

Received: 7 May 2009 / Accepted: 30 June 2009 / Published online: 16 July 2009

Abstract In this study, ZnO nanostructures with different morphologies including nanorods, nanowires, and nanobrushes were synthesized by a simple hydrothermal process without using any structure-directing reagent. The samples were characterized by X-ray diffraction, field emission scanning electron microscopy, and transmission electron microscopy. The influence of the preparation parameters on the morphology of ZnO is discussed. Gas-sensing properties of the materials were investigated. The results reveal that all the prepared nanostructured ZnO powders show high response to ethanol, among which, the three-dimensional nanobrushes show the highest response, demonstrating excellent potentiality for ethanol sensors.

Introduction

Zinc oxide (ZnO) is an extensively studied material owing to its non-toxicity, inexpensive production, easy to grow nature, and more importantly, to its multifunction. ZnO is of interest for potential applications in optoelectronic devices such as solar cells [1], field emission displays [2], sensors [3], and other devices [4, 5] due to its wide direct-band gap (3.37 eV) and large exciton-binding energy of 60 meV. ZnO is an important semiconductor for sensing toxic and combustible gases. In short, ZnO sensors hold a large variety of advantages, such as low cost, short response time, easy manufacturing, and small size, compared to the traditional analytical instruments. However, its working temperature is rather high, normally at 400–500 °C, and selective response is fairly poor. Nowadays, efforts have been made on improving preparation methods to synthesize ZnO with different morphologies for sensors with low working temperature. Ethanol-sensing properties of one-dimensional (1D) nanostructures such as nanorods [6–9], nanowires [10], and nanotubes [11] have been widely investigated, while gas-sensing properties of three-dimensional (3D) hierarchical ZnO nanostructures been rarely investigated. Recently, brush-like hierarchical ZnO nanostructures based on individual nanorods have shown very good ethanol gas-sensing properties at 265 °C [12]. However, the gas-sensing properties of 3D nanobrushes assembled from flower-like ZnO nanorods have not yet been investigated.

Morphology control is considerably important in manufacturing ZnO nanostructures for specific purpose. In many applications, both size and shape play important roles in determining the properties and the utilities of the nanomaterials. For ZnO nanostructures, investigations have been focused on the synthesis and characterization of intrinsic ZnO, especially on 1D and 3D ZnO nanostructures. In the past decade, 1D ZnO and 3D hierarchical nanostructures, such as nanorods, nanowires, nanotubes, nanoribbons, and nanobrushes, have been successfully prepared in laboratories. 1D and 3D hierarchical ZnO nanostructures can be synthesized by various methods including thermal evaporation [13], pulsed-laser deposition [14], electrochemical deposition [15], sonochemical method [16], sol–gel [17], and hydrothermal synthesis with surfactants or other organic compounds as capping or directing reagents [18–20]. However, these preparation methods are often limited in practical applications due to low yields and rigorous reaction conditions, such as high temperature, long reaction time, and use

W.-D. Zhang (✉) · W.-H. Zhang · X.-Y. Ma
Nano Science Research Center, School of Chemistry and Chemical Engineering, South China University of Technology, 381 Wushan Road, Guangzhou 510640, People's Republic of China
e-mail: zhangwd@scut.edu.cn

of toxic template, complex equipment, etc. Thus, it is imperative to explore a simple, low-cost, environmentally friendly, and high-yield synthetic method for the preparation of ZnO nanostructures. Herein, we report a facile approach for size-controlled synthesis of ZnO nanostructures including nanorods, nanowires, and nanobrushes by hydrothermal process at the low temperature of 90 °C. Their gas-sensing properties are also investigated.

Experimental section

Preparation and characterization of ZnO

ZnO was prepared by a simple hydrothermal method. A solution saturated with $Zn(OH)_4^{2-}$ for hydrothermal synthesis of ZnO was prepared by dissolving ZnO (Aldrich, 99.5%) in a 5-M NaOH solution. Different ZnO nano-/micro-structures were synthesized by controlling the volume ratio of the ZnO-saturated 5-M NaOH solution, NaOH solution, and water.

S1 and S2 were prepared with the ratio $[V_{Zn(OH)_4^{2-}}/V_{NaOH}/V_{H_2O}]$ of 3:0:37 and 1:2:37, respectively, i.e., S1 was prepared by adding 3 mL of the ZnO-saturated 5-M NaOH solution to 37-mL distilled water; while S2 was prepared by mixing 2 mL of the 5-M NaOH solution, 1 mL of the ZnO-saturated solution, and 37-mL distilled water under constant stirring. The resulting solution was transferred into a 50-mL Teflon-lined stainless steel autoclave and sealed tightly. The pH value of the resulting solution was about 13.5 and 14.0 for the preparation of samples S1 and S2, respectively. Hydrothermal treatment was carried out at 90 °C for 10 h. After that, the autoclave was allowed to cool down naturally.

The mixture solution for the synthesis of S3 was the same as that for S1, i.e., a mixture of 3 mL of ZnO-saturated solution and 37-mL distilled water, while 0.01-g S1 powder was dispersed in the mixture solution by ultrasonication for 30 min. The resulting suspension was then heated at 90 °C for 10 h.

S4 was prepared at room temperature (about 25 °C) by mixing 1-mL ZnO-saturated 5-M NaOH solution with 37-mL distilled water in a 100-mL beaker for 15 min and white precipitate was formed. The pH value of the resulting solution was about 12.5 for the preparation of sample S4.

The prepared precipitates were separately collected, washed with distilled water several times, and then dried at 100 °C overnight.

The crystal structures of the resulting products were characterized by a Shimadzu XD-3A X-ray diffractometer (XRD) with Cu Kα radiation ($\lambda = 1.5406$ nm). XRD patterns were recorded from 10° to 70° at a scan rate of 4° min^{-1}. A field emission scanning electron microscope (FESEM) (JEOL JSM 6700F) was used to observe ZnO samples. Transmission electron microscopy (TEM) observation was performed with a Philips CM 300 FEG instrument operated at 300 kV. The Brunauer–Emmett–Teller (BET) surface area was determined by a ST-08A measuring instrument (Beijing Analysis Instruments Technical Company, Beijing, China).

Fabrication and evaluation of the gas sensors

Details of gas-sensing measurement were operated as reported in Ref. [21]. The powder samples were dry-ground and then wet-ground with a terpineol solution to form a paste, respectively. The paste was coated onto an Al_2O_3 tube with two gold leads at each end. After dried in air, it was sintered at 600 °C for 2 h. Finally, the electrodes were fixed on the circuit for measurement. A heater using Ni–Cr wire was inserted into the Al_2O_3 tube to supply the necessary operation temperature. Resistance of the sensor was measured in air and in sample gases, respectively. A chamber was filled with air at 101.3 kPa, and then ethanol was injected into the chamber. The gas concentration in the chamber was calculated according to the amount of ethanol injected and the chamber volume. The response (S) was defined as the ratio (R_a/R_g) of the resistance in air (R_a) and in a sample gas or vapor (R_g). The response/recovery time was defined as the time to reach 90% of the final change in resistance, when the gas was turned on or off, respectively.

Results and discussion

Crystal structure and morphology of the prepared ZnO

The XRD patterns of the as-synthesized ZnO samples are displayed in Fig. 1. All the samples show well-crystallized

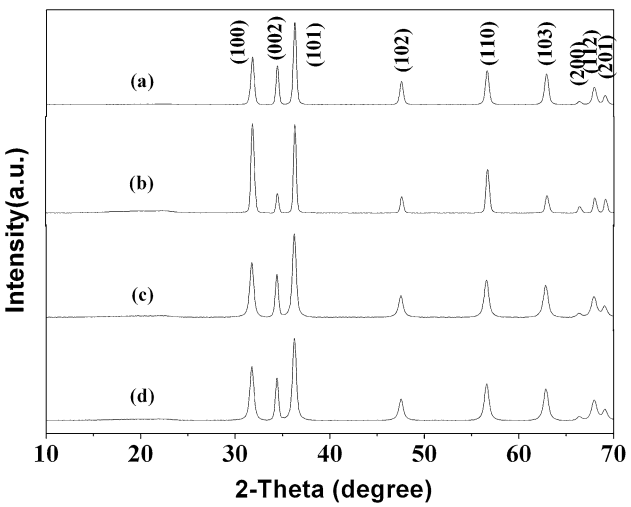

Fig. 1 XRD patterns of (a) S1, (b) S2, (c) S3, and (d) S4

diffraction peaks, and the absence of impurity peak suggests high purity of the prepared samples. All the diffraction peaks are well indexed to the standard hexagonal ZnO crystal (JCPDS 36-1451).

The morphologies of the synthesized ZnO in various conditions were visualized by SEM, as depicted in Fig. 2. Uniform flower-like ZnO, which consists of many hexagonal nanorods with smooth surfaces, is observed in Fig. 2a. The diameter and the length of S1 are about 300 nm and 2.4 μm, respectively. Inset in Fig. 2a shows the zoom-in observation on the right corner. One can see a hexagonal nanorod with other six hexagonal nanorods attached on each side near the root. Each nanorod is almost the same size and shape, and is with a sword-like tip. When the ratio $[V_{Zn(OH)_4^{2-}}/V_{NaOH}/V_{H_2O}]$ being changed to 1:2:37, the obtained ZnO is also flower-like, but the 1D ZnO is much thinner, grown to be needle-like nanowires (Fig. 2b). The diameter and the length of S2 are about 300 nm and 10 μm, respectively. It is very interesting that ZnO nanowires can grow from the sidewalls of the nanorods by another hydrothermal process. As shown in Fig. 2c and d, the morphology of S3 is nanobrushes and these ZnO nanobrushes are composed by many small nanowires growing on every nanorod, forming hierarchical structure. Additionally, the size and shape of the original nanorods is not changed.

The formation of self-assembly ZnO nanostructures in aqueous solution could be explained by the homogeneous and heterogeneous nucleus mechanism [22, 23]. The overall reaction procedure for growing 1D ZnO nanostructures in an aqueous alkaline solution is proposed below:

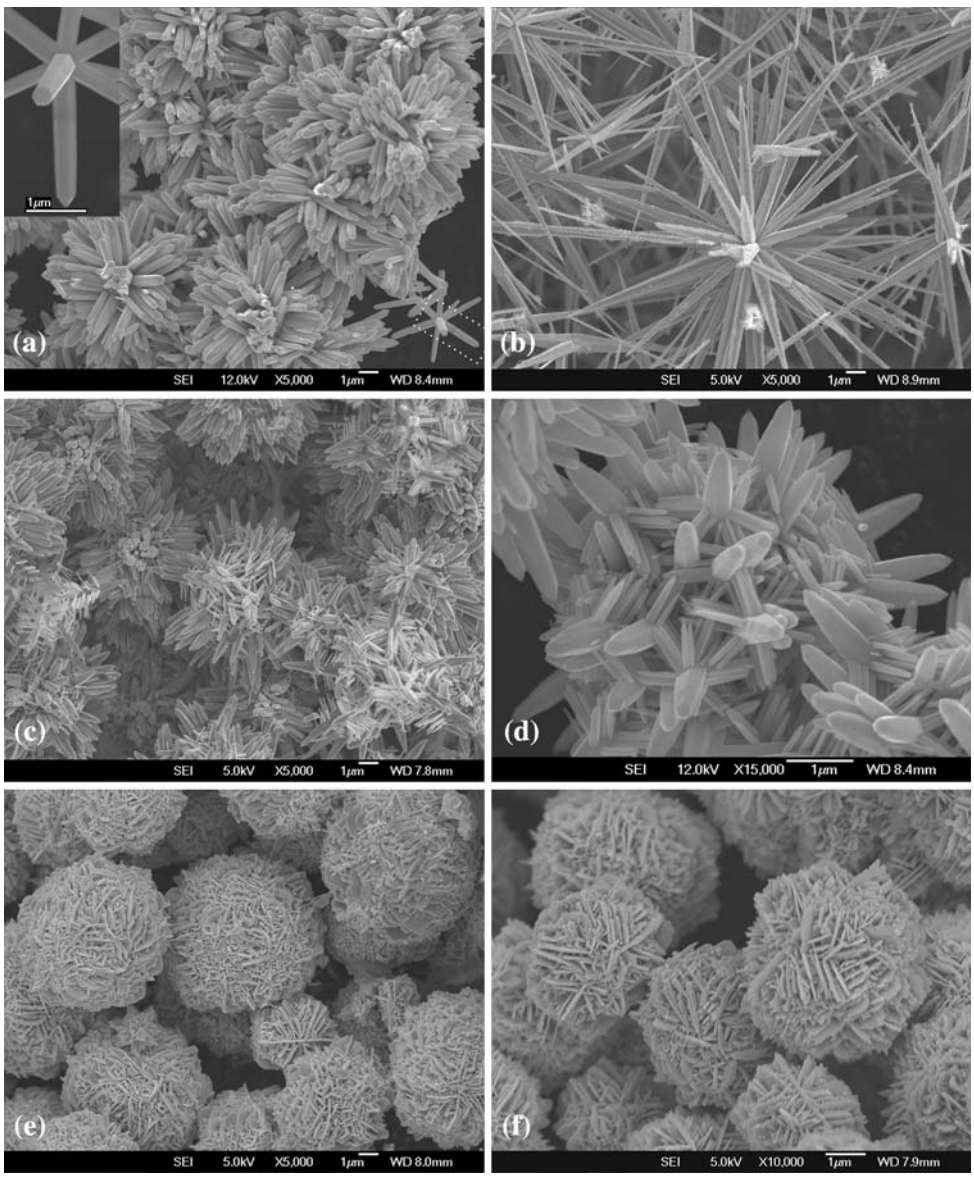

Fig. 2 FESEM images of **a** S1; **b** S2; **c**, **d** S3; and **e**, **f** S4

$$ZnO + 2OH^- + H_2O \rightarrow Zn(OH)_4^{2-} \quad (1)$$

$$Zn(OH)_4^{2-} \rightarrow ZnO + H_2O + 2OH^- \quad (2)$$

A solution saturated with $Zn(OH)_4^{2-}$ for hydrothermal synthesis of ZnO nanorods or nanowires was prepared by dissolving commercial ZnO powders in a 5-M NaOH solution. The above saturated solution was diluted to different concentrations with H_2O. At an early stage, initially grown ZnO nuclei from the decomposition of $Zn(OH)_4^{2-}$, acted as seeds. The newly formed species adsorbed onto them enhanced the anisotropic growth, resulting in the formation of nanorods. Under the aqueous alkaline condition, polar growth of ZnO crystal along the [001] directions proceeds through the adsorption of growth units of $Zn(OH)_4^{2-}$ onto the (001) plane, resulting in an anisotropic growth [22]. The growth of ZnO nanowires could be attributed to the low concentration of $Zn(OH)_4^{2-}$ solution during the hydrothermal process. The thickness of the nanorods could be tuned by varying the concentration of $Zn(OH)_4^{2-}$ solution, but the pH value of the solution must be kept at 13.5 or higher. ZnO nanorods can also act as the heterogenous nuclei sites for the adsorption of newly formed species from the decomposition of $Zn(OH)_4^{2-}$, and then epitaxially grow on the nanorods along the six sidewalls to be nanowires [20], resulting in the formation of ZnO nanobrushes with 6-fold symmetry configuration [Fig. 2c, d; 23–25]. It is worth pointing out that we can prepare ZnO nanorods and nanowires in large amount by this hydrothermal process using large volume autoclaves. The pH value of the solution is critically important for the growth of ZnO nanorods or nanowires. The pH values of the solutions for the synthesis of nanorods and nanowires were adjusted to about 13.5. Otherwise, ZnO microparticles were formed soon at room temperature. As shown in Fig. 2e, the morphology of S4 is microparticles which seem to be consists of aggregates of nanoplatelets (Fig. 2f). The mean grain size was 5 μm. Our experimental results obviously indicate that the thickness of the 1D ZnO can be controlled by varying the concentration of $Zn(OH)_4^{2-}$ with maintaining pH of 13–14.

Further insight into the detailed structure and morphologies of the products were gained by TEM analysis, as indicated in Fig. 3. The flower-like structure of S1 is depicted in Fig. 3a, which is consistent with SEM

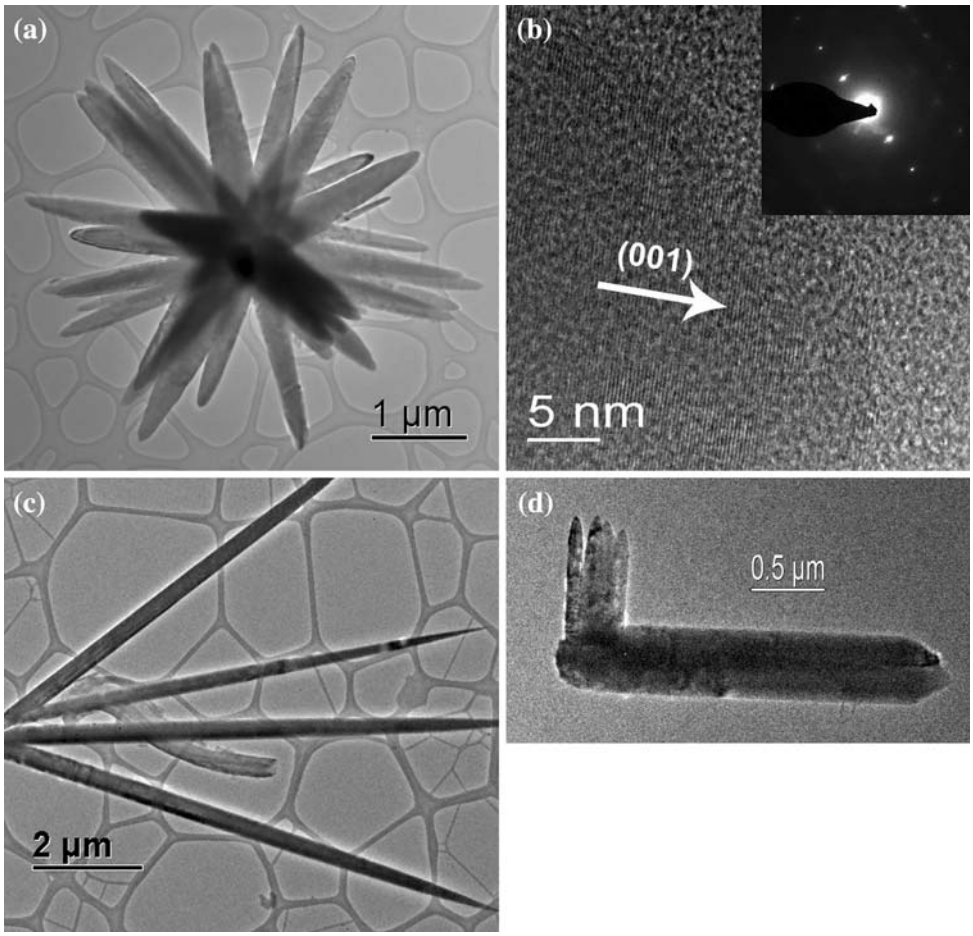

Fig. 3 TEM images of **a**, **b** S1; **c** S2; and **d** S3

observation. The HRTEM image of a nanorod shown in Fig. 3b clearly indicate the fringes corresponding to the (001) planes of hexagonal ZnO. The growth direction of nanorods can be indexed to [001] direction. The nanorods are single crystal [26]. Figure 3c shows the thinner ZnO nanowires prepared in diluted $Zn(OH)_4^{2-}$ solution. The brush-like hierarchical structure of S4 is depicted in Fig. 3d. One can see several nanowires attached on a nanorod. The average diameter and the length of nanowires grown on the nanorod are about 90 nm and 850 nm, respectively.

Gas-sensing properties of the prepared samples

Gas-sensing properties of the prepared samples with different morphologies were studied. In general, gas sensors are affected by the working temperature. Response of the ZnO sensors to 50 ppm ethanol at 150–330 °C is illustrated in Fig. 4. Upon increase of the working temperature, the response of S1, S2, and S4 sensors to 50 ppm ethanol all increased from 150 to 270 °C and reached the maximum of 9.2, 7.1, and 16.5 at 270 °C, respectively. However, the response of S3 sensor increased from 150 to 240 °C and reached the maximum of 23 at 240 °C. The working temperature was controlled at 240 °C for testing the performance of the sensors. In addition, one can see from Fig. 4 that the nanowires (sample S2) exhibited the lowest response at the testing temperature ranging from 150 to 270 °C, and effect of temperature on the response of the nanorods (sample S1) was limited.

The response/recovery time is an important parameter for characterizing sensors. The response/recovery time of the ZnO sensors to 50 ppm ethanol at 240 °C is summarized in Table 1. The response time of S1, S3, and S4

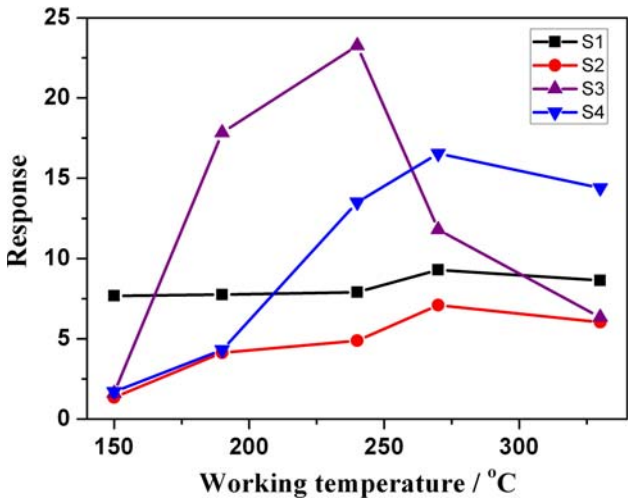

Fig. 4 Response of ZnO sensors to 50 ppm ethanol at different working temperature

Table 1 Response/recovery time of sensors at 240 °C

Sample number	S1	S2	S3	S4
Response time/s	14	37	16	15
Recovery time/s	38	49	56	59

sensors was less than 18 s, while the response time of S2 sensor was 37 s. The recovery time of all the ZnO sensors was less than 60 s. All the four sensors based on ZnO nano-/micro-structures show rapid response and recovery.

The gas-sensing mechanism of ZnO-based sensors belongs to the surface-controlled type. Its response is relative to grain size, surface state, oxygen adsorption quantity, active energy of oxygen adsorption, and lattice defects. Normally, the smaller its grain size is, the higher its response is; the higher specific surface area and oxygen adsorption quantity are, the higher its response is [27, 28]. The absorbed oxygen captures free electrons, thus reducing the conductance of ZnO. When ZnO is exposed to a reducing gas (ethanol in our case), the ethanol molecules react with the absorbed oxygen. This process causes the release of electrons from the oxygen ions, thus increases the conductance. 1D ZnO nanostructures have a loosely packed structure, which provides larger channels or pores, and a higher surface area than the film of spherical or granular particles, which are usually aggregated tightly when being sintered to be films for fabricating sensors [29]. 1D ZnO nanostructures are favorable for conducting the charge induced when being exposed to the sample gases or vapors, and target gas molecules can access the inner of the 1D nanostructures film as well. The gas-sensing properties of 1D ZnO nanostructures are affected by the morphology and size. S1 sensor based on ZnO nanorods showed better gas-sensing properties than S2 sensor based on ZnO nanowires. It is noticed that the specific surface area of the ZnO nanorods (0.5 $m^2\ g^{-1}$) is smaller than that of nanowires (2.1 $m^2\ g^{-1}$), while the aspect ratio of the nanorods is lower than that of the nanowires. Therefore, the sensing element based on nanorods may induce more cavities that allow the target gas molecules to access the inner of nanorods film quickly. S3 sensor based on ZnO nanobrushes, a combination of the nanorods and nanowires, showed better gas-sensing properties than S1 sensor and S2 sensor. The improved ethanol gas-sensing performance of ZnO nanobrushes over that of nanorods and nanowires may be attribute to (1) the nanobrushes structures improve specific surface area (19.6 $m^2\ g^{-1}$) and (2) the nanobrushes structures form a film with more cross-linking structure that allows the gas molecules to diffuse deeply into the film. It is very interesting that the microparticles with nanofolds on the surface also exhibited good response to ethanol. This could also be attributed to the larger surface area

($13.3\ m^2\ g^{-1}$) because of the hierarchical structure on the surface of the microparticles. More details of gas-sensing properties of the ZnO nanostructures need further investigation.

Conclusion

In summary, morphology-controlled ZnO nanostructures including nanorods, nanowires, and nanobrushes were successfully synthesized through controlling the preparation parameters by hydrothermal process without any organic additive. Sensors based on the hierarchical ZnO nanomaterials, including nanobrushes and microparticles with folds on the surface showed higher response to ethanol at 240 °C, demonstrating the potential application of the ZnO nanostructures for ethanol sensors with high performance.

Acknowledgements The financial support of this study is by the Research Fund for the Doctoral Program of Higher Education (RFDP) under Grant 20070561008 and Natural Science Foundation of China under Grant 20773041 is greatly acknowledged.

References

1. Hara K, Horiguchi T, Kinoshita T, Sayama K, Sugihara H, Arakawa H (2000) Sol Energy Mater Sol Cells 64:115
2. Dong L, Jiao J, Tuggle DW, Petty JM, Elliff SA (2003) Appl Phys Lett 82:1096
3. Zhu BL, Xie CS, Wang AH, Wu J, Wu R, Liu J (2007) J Mater Sci 42:5416. doi:10.1007/s10853-006-0768-2
4. Agarwal G, Speyer RF (1998) J Electrochem Soc 145:2920
5. Kind H, Yan H, Messer B, Law M, Yang P (2002) Adv Mater 14:158
6. Xu JQ, Chen YP, Chen DY, Shen JN (2006) Sens Actuators B 113:526
7. Xu JQ, Chen YP, Li YD, Shen JN (2005) J Mater Sci 40:2919. doi:10.1007/s10853-005-2435-4
8. Liao L, Lu HB, Li JC, He H, Wang DF, Fu DJ, Liu C (2007) J Phys Chem C 111:1900
9. Rout CS, Krishna SH, Vivekchand SRC, Govindaraj A, Rao CNR (2006) Chem Phys Lett 418:586
10. Hsueh TJ, Hsu CL, Chang SJ, Chen IC (2007) Sens Actuators B 126:473
11. Chen YJ, Zhu CL, Xiao G (2008) Sens Actuators B 129:639
12. Zhang Y, Xu JQ, Xiang Q, Li H, Pan QY, Xu PC (2009) J Phys Chem C 113:3430
13. Zhang ZQ, Jiang CB, Li SX, Mao SX (2008) J Cryst Growth 277:321
14. Tien LC, Pearton SJ, Norton DP, Ren F (2008) J Mater Sci 43:6925. doi:10.1007/s10853-008-2988-0
15. Zheng MJ, Zhang LD, Li GH, Shen WZ (2002) Chem Phys Lett 363:123
16. Wahab R, Ansari SG, Kim YS, Seo HK, Shin HS (2007) Appl Surf Sci 253:7622
17. Li J, Srinivasan S, He GN, Kang JY, Wu ST, Ponce FA (2008) J Cryst Growth 310:599
18. Kale RB, Lu SY (2007) J Phys: Condens Mater 19:096209
19. Zhang TR, Dong WJ, Brewer MK, Konar S, Njabon RN, Tian ZR (2006) J Am Chem Soc 128:10960
20. Gao XP, Zheng ZF, Zhu HY, Pan GL, Bao JL, Wu F, Song DY (2004) Chem Commun 12:1428
21. Zhang WH, Zhang WD (2008) Sens Actuators B 134:403
22. Li WJ, Shi EW, Zhong WZ, Yin ZW (2008) J Cryst Growth 203:186
23. Sounart TL, Liu J, Voigt JA, Huo M, Spoerke ED, McKenzie B (2007) J Am Chem Soc 129:15786
24. Sounart TL, Liu J, Voigt JA, Hsu JWP, Spoerke ED, Tian Z, Jiang YB (2006) Adv Funct Mater 16:335
25. Lao JY, Wen JG, Ren ZF (2000) Nano Lett 2:1287
26. Zhang WD (2006) Nanotechnology 17:1036
27. Xu JQ, Pan QY, Shun YA, Tian ZZ (2000) Sens Actuators B 66:277
28. Lv YZ, Guo L, Xu HB, Chu XF (2007) Physica E 36:102
29. Si SF, Li CH, Wang X, Peng Q, Li YD (2006) Sens Actuators B 119:52